Deformation studies at high spins in γ-soft ^{179}Re nucleus

S. K. Chamoli,[1] P. Joshi,[1,2] A. Kumar,[1] G. Singh,[1] R. P. Singh,[2] S. Muralithar,[2] R. K. Bhowmik,[2] L. Chatturvedi,[3] Z. Naik,[4] C. R. Praharaj,[4] and I. M. Govil[1]

[1]*Department of Physics, Panjab University, Chandigarh-160014, India*
[2]*Nuclear Science Centre, Post Box No. 10502, New Delhi-110067, India*
[3]*Department of Physics, Banaras Hindu University, Varanasi, India*
[4]*Institute of Physics, Bhubneshwar-751005, India*

(Received 24 June 2003; published 5 March 2004)

The nuclear shape studies are done for different quasiproton bands in ^{179}Re nucleus through lifetime measurement using recoil distance Doppler shift technique. The deformation driving property of the low K, $h_{9/2}[541]1/2^-$ intruder band and the stretching property of the high K, $d_{5/2}[402]5/2^+$ and $h_{11/2}[514]9/2^-$ bands are discussed. The average quadrupole moment obtained from these measurements for the $h_{9/2}$ configuration ($Q_t \sim 6.5$ e b) is found to be about 16% higher than the average quadrupole moment ($Q_t \sim 5.6$ e b) for the $d_{5/2}$ and the $h_{11/2}$ configurations. The higher value of quadrupole moment for the low $K=1/2$, $h_{9/2}$ band as compared to the high $K=9/2$, $h_{11/2}$, and $K=5/2$, $d_{5/2}$ bands indicates its deformation driving property. The cranked Hartree-Fock-Bogoliubov and the microscopic Hartree-Fock calculations are done for these bands and are compared with the experimental observations.

DOI: 10.1103/PhysRevC.69.034310 PACS number(s): 21.10.Tg, 21.10.Ky, 27.70.+q

I. INTRODUCTION

The lifetime measurements of the odd-Z nuclei around $A \sim 180$ are important to study the shape driving effects of the various single-particle orbitals on the even-even core and the other correlated phenomena. In this respect the study of the rhenium nuclei may be instructive as they fall on the outer edge of the well deformed rare earth nuclei and are γ soft because of the shape driving forces. For the Re nuclei the strongly decoupled $\pi h_{9/2}[541]1/2^-$ orbital is above the Fermi level and hence acts as a particle state while the strongly coupled $\pi d_{5/2}[402]5/2^+$ and $\pi h_{11/2}[514]9/2^-$ orbitals are below the Fermi level and hence act as hole states. When the odd proton of the Re nuclei occupies the highly downsloping $\pi h_{9/2}[541]1/2^-$ orbital then it has a strong effect on driving the even-even nuclear core to large β_2 and positive γ deformations. On the other hand when the odd proton occupies the upsloping $\pi d_{5/2}[402]5/2^+$ and $\pi h_{11/2}[514]9/2^-$ orbitals then it has a tendency to drive the nuclear core towards spherical shapes. Thus excitation of an odd particle to any of these configurations presents the possibility of examining the effects on the collectivity and the associated nuclear shapes. The shape driving property of these intruder single-particle orbitals for the rare earth nuclei has been comprehensively studied by Jin *et al.* [1]. The lifetime measurements in ^{171,173}Ta, ^{177}Re, and ^{179}Ir [2–5] nuclei have confirmed the deformation driving properties of these single-particle orbitals, and the delay of $\sim$70 keV observed in the band crossing frequency for this low $K(1/2)$ $\pi h_{9/2}$ band as compared to the band crossing frequency for the ground state band in the nearest even-even neighbors and also compared to the other bands in these nuclei is interpreted as because of the higher deformation for this band. As the deformation in these nuclei is caused by the collective motion of the nucleons outside the closed shell, so it is expected to increase as one moves away from the closed shell at $N=82$ to the midshell at $N=104$ and then decreases again towards the next closed shell at $N=120$, thus forming a deformation plateau near the midshell. The deformation measurements in ^{179}Re nucleus are interesting as it has 104 neutrons corresponding to neutron midshell and therefore it is expected to possess the maximum deformation. Also on observing the nature of the AB neutron band crossing for different bands in rhenium nuclei a strong and irregular variation of band crossing with the neutron number is observed. The $[541]1/2^-$ band shows a backbending in ^{177}Re [6] but forward bending in ^{179}Re [7]. The $[402]5/2^+$ and $[514]9/2^-$ bands on the other hand display forward bending in ^{177}Re and upbending in ^{179}Re. This is a puzzling result and may be associated with either the shape changes or the level density effects. In order to have a clear understanding of the variation of the band crossing behavior with neutron number in these nuclei, it is important to measure the deformation of different bands in ^{179}Re nucleus. As the lifetime measurements of the excited nuclear states provide key information on the quadrupole deformation of different configurations, we have done the lifetime measurements for different bands in ^{179}Re using recoil distance Doppler shift technique (RDM). Part of the results of this paper for the $h_{9/2}$ ($K=1/2$) and $d_{5/2}$ ($K=5/2$) bands has already been presented in ISPUN02 conference in Vietnam [8]. However the results for the $h_{11/2}$ ($K=9/2$) band are newly presented. The results are compared with the microscopic Hartree-Fock calculations for the first time in this paper.

II. EXPERIMENTAL DETAILS

The nucleus ^{179}Re was populated by the fusion evaporation reaction ^{165}Ho(^{18}O,$4n$)^{179}Re with oxygen beam at 82 MeV delivered by the 15 UD pelletron at Nuclear Science Center (NSC), New Delhi. Self-supporting ^{165}Ho target of thickness 800 μg/cm^2 and the gold stopper of thickness

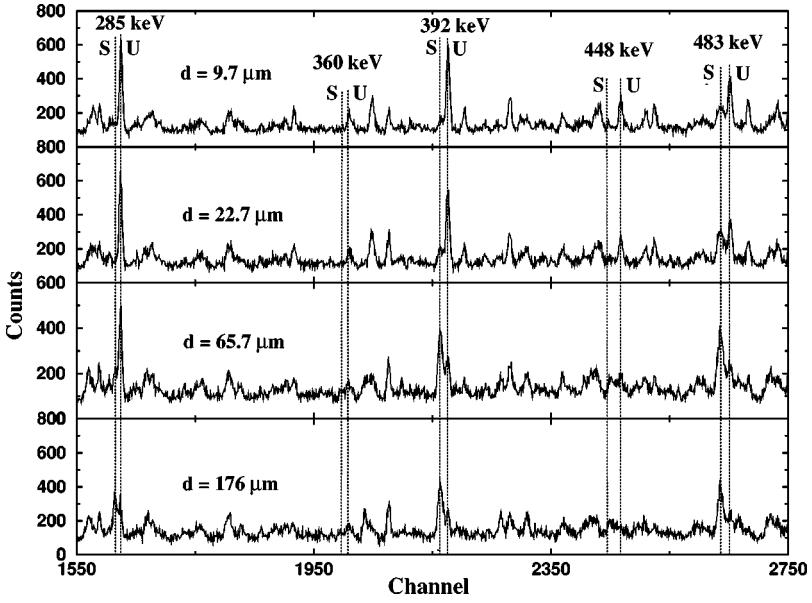

FIG. 1. The shifted (S) and the unshifted (U) peaks of γ transitions in ^{179}Re at four different target-stopper distances ($D_{T\text{-}S}$) at an angle of 144° with respect to the beam direction.

8 mg/cm^2 were used in the reaction. The recoil distance plunger device in combination with the gamma detector array consisting of 12 HPGe detectors was used for this experiment. The distance between the target and the stopper was measured using the capacitance method [9]. The data were acquired for 18 target to stopper distances ($D_{T\text{-}S}$) ranging from 10 to 5000 μm. The γ rays were detected with 12 Compton supressed HPGe detectors arranged in three different rings of four detectors each, making an angle of 144°, 98°, and 50° with respect to the beam direction. A 14-elements bismuth germanate (BGO) multiplicity detector array was used to reduce the background due to the radioactivity and the Coulomb excitation, etc. The data are acquired in the coincidence mode (γ-γ) and also in the singles mode with the γ multiplicity condition that at least two BGOs should fire in coincidence with one Ge detector. As the statistics in the coincidence mode (γ-γ) was not enough, the singles data with the BGO multiplicity filter ($M \geqslant 2$) were used for the analysis. The four HPGe detectors at a particular angle were gain matched, added, and used for the lifetime measurements. The typical singles spectra at four target-stopper ($D_{T\text{-}S}$) distances with the shifted and the unshifted peaks for a few γ-ray energies of our interest are shown in Fig. 1. The shifted and the unshifted γ-ray peaks were clearly separated up to spin $33/2^-$, $25/2^-$, and $19/2^+$ for the $h_{9/2}$, $h_{11/2}$, and the $d_{5/2}$ bands, respectively. The γ rays from the higher transitions in these bands were either fully shifted or were not resolved from the background due to the poor statistics.

III. DATA ANALYSIS AND RESULTS

The decay curves of the unshifted intensity as a function of the target-stopper distance were used for the lifetime analysis. The intensity normalization was done with the total intensity (sum of the shifted and the unshifted intensity) and also done with 547 keV Coulomb excited gold peak. The fitting of these decay curves and the extraction of the lifetimes were done using the computer code LIFETIME [10] which takes into account the problem of side feeding by direct solution of the Bateman equations and applies all the other necessary corrections required in the raw data such as correction for the change in solid angle due to the motion of recoils, for finite target thickness and for the loss of total γ-ray intensity caused by the changes in the angular distribution of the γ rays due to the deorientation effect. The angular distribution of γ rays emitted from aligned nuclei can be given by

$$W(t) = 1 + A_2(t)P_2(\cos\,\theta) + A_4(t)P_4(\cos\,\theta), \qquad (1)$$

where A_2 and A_4 are the angular distribution coefficients and P_2 and P_4 are Legendre polynomials. According to Abragam and Pound [11] treatment of attenuation of alignment, A_2 and A_4 vary exponentially in the following way

$$A_2(t) = A_{20}\, e^{t/\tau_2}, \quad A_4(t) = A_{40}\, e^{t/\tau_4}, \qquad (2)$$

where the coefficients A_{20}=0.368 and A_{40}=−0.112 and τ_2 and τ_4 are the electronic relaxation times taken as 30 ps and 10 ps, respectively. The intensity of the side feedings is assumed by the program so that the total γ-ray intensity is balanced within the band under consideration. The transition rates of the unknown side feedings are taken as free parameters and adjusted to have the best fit of the experimental data. The initial populations and transition rates of the γ-ray transitions within the band are adjusted by the program MINUIT [12] included in the LIFETIME code to calculate the true parameter errors. It includes the statistical error and the errors arising from the correlation among different parameters. The correlated uncertainties from the fitting process were estimated by examining the behavior of χ^2 function over the unit interval on both sides of the minimum.

The decay curves for the unshifted γ transitions in the $h_{9/2}$, $d_{5/2}$, and $h_{11/2}$ bands are shown in Figs. 2, 3, and 4, respectively. The results of the lifetime measurements for these bands are tabulated in Tables I–III, respectively. From the measured lifetimes, the reduced transition probability

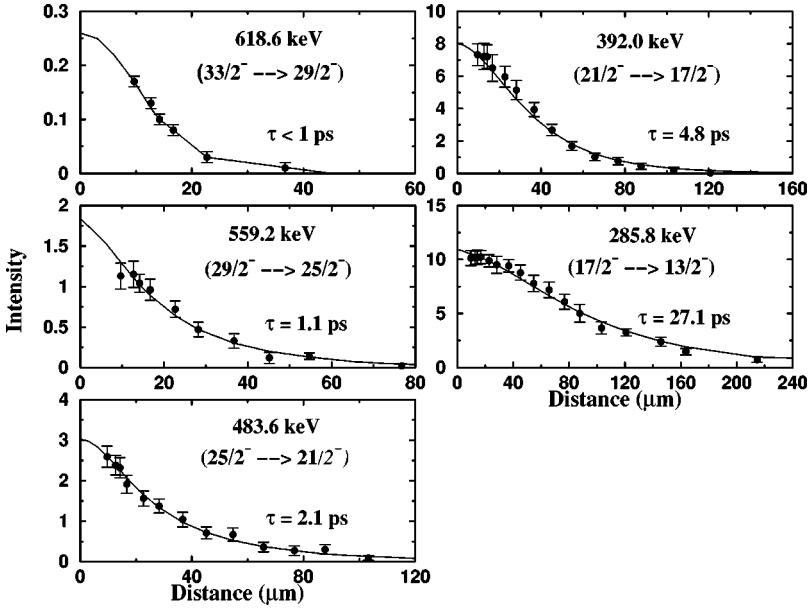

FIG. 2. The intensity decay curves for the unshifted γ-ray transitions in the $\pi h_{9/2}[541]1/2^-$ band in ^{179}Re.

$B(E2)$ and the reduced transition quadrupole moment Q_t have been extracted using the following relations:

$$T(E2) = [1.23 \times (10)^{13}](E_\gamma)^5 B(E2) \tag{3}$$

and

$$B(E2; I \rightarrow I-2) = \left(\frac{5}{16\pi}\right)\langle I\ 2\ K\ 0|I-2K\rangle^2\ Q_t^2, \tag{4}$$

where $T(E2)$ is the transition rate in unit of $(\text{sec})^{-1}$, $B(E2)$ in units of e^2 b^2, and Q_t is in the unit of e b. The reduced transition probabilities $B(E2)$ and the quadrupole moments Q_t for all three bands are tabulated in Tables I–III.

A. Total Routhian surfaces (TRS) calculations

To have a better understanding of the deformation properties of the negative parity $h_{9/2}[541]1/2^-$ and the positive parity $d_{5/2}[402]5/2^+$ ground state bands in ^{179}Re, we have carried out the TRS calculations [13] with Strutinsky shell correction procedure [14]. The axial Wood-Saxon potential [15] with quadrupole β_2 and hexadecapole β_4 deformations is used in the calculations as the mean field. The residual interaction is assumed to be of monopole type [16] while the pair gap Δ and the chemical potential λ are calculated using the BCS self-consistence method. The total Routhian surfaces are minimized with respect to the deformation parameters β_2, β_4, and γ and the resulting TRS contours are plotted in the β_2-γ plane at different rotational frequencies. Using the deformation parameters obtained from the TRS calcula-

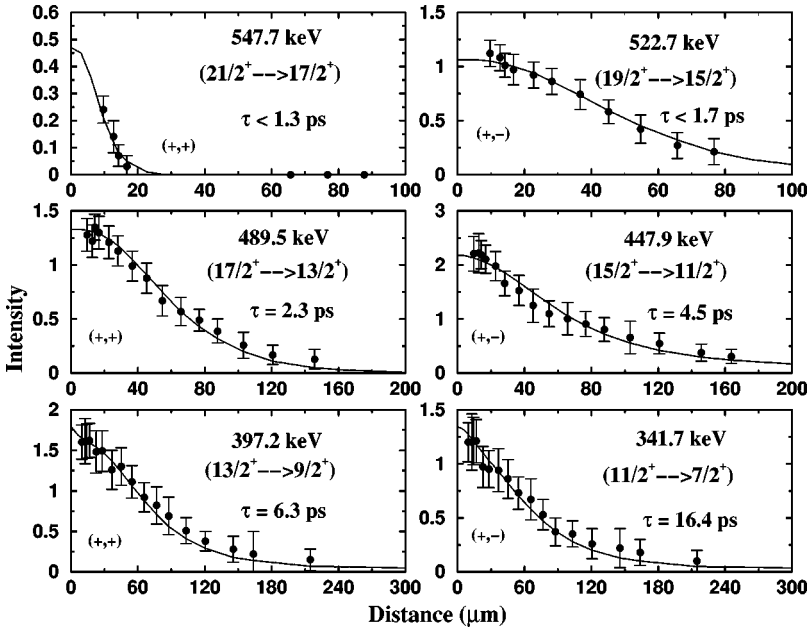

FIG. 3. The intensity decay curves for the unshifted γ-ray transitions of both signature partners in $\pi d_{5/2}[402]5/2^+$ band in ^{179}Re.

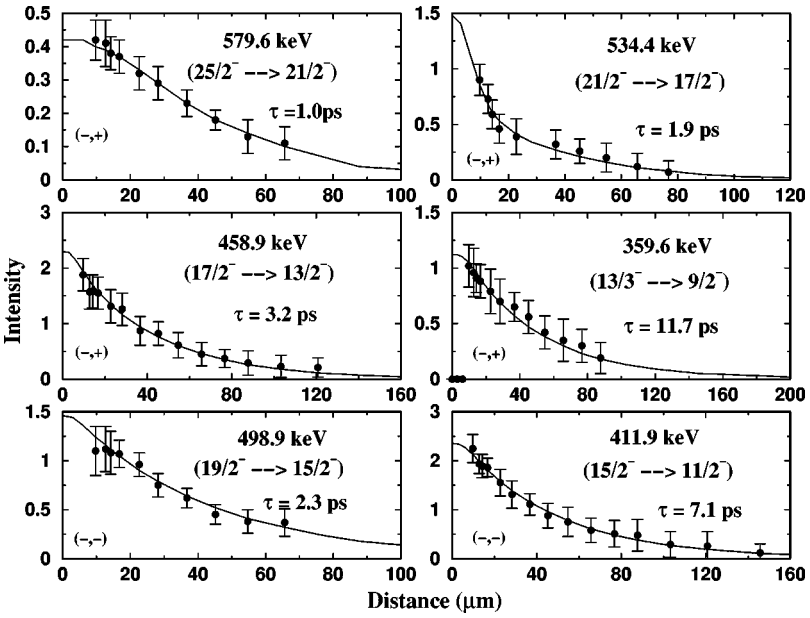

FIG. 4. The intensity decay curves for the unshifted γ-ray transitions of both signature partners in $\pi h_{11/2}[514]9/2^-$ band in ^{179}Re.

tions the theoretical Q_t values are computed using the following relation, where "Ze" is the charge on the nucleus and the radius $r_0=1.2$ fm:

$$Q_t = \frac{6}{\sqrt{15\pi}} Ze\, r_0^2\, A^{2/3} \beta_2 (1 + 0.36\beta_2) \cos(30^\circ + \gamma). \quad (5)$$

At differential rotational frequencies, the calculated β_2, γ, and Q_t values are tabulated in Table IV for the negative parity ($\alpha = +1/2$) and positive parity ($\alpha = \pm 1/2$) bands. The calculations show almost no change in the quadrupole deformation as a function of the rotational frequency, which is consistent with the experimental observations.

B. Shape studies with microscopic Hartree-Fock and angular momentum projection technique

The observed rotational bands in ^{179}Re are also studied in a microscopic way by the projection of total angular momentum from deformed intrinsic states and by subsequent diagonalization. Axial symmetry of the Hartree-Fock field is assumed in the calculations. For the calculations the nuclear Hamiltonian [17–19] is considered to be the sum of the single-particle energy term "ϵ" and the residual two-body interaction potential term "V, i.e.,

$$H = \epsilon + V, \quad (6)$$

where V consists of V_{pp}, V_{pn}, and V_{nn} interaction terms. A surface δ residual interaction [20], which gives reasonable deformation properties in this mass region, of strength $F_{pp} = F_{pn} = F_{nn} = 0.157$ MeV is used in the calculations. Hartree-Fock (HF) orbits are calculated with a spherical noninteracting closed shell core of $Z=50$ and $N=82$ with one major shell active each for protons and neutrons. The orbits of the model space with respective single-particle energies used for HF orbits and angular momentum projected spectra calculations are given in Table V along with the values of the proton and neutron effective charges.

Intrinsic states $K=9/2^-$,$K=5/2^+$ are obtained by suitable odd proton occupation near the Fermi surface. For the $K=1/2^-$ configuration, the odd proton occupies $\Omega=1/2^-$ orbit (mostly of $h_{9/2}$ origin) well above the Fermi surface.

A deformed HF orbit with axial symmetry is in general a superposition of various j states. One has

$$|\alpha m\rangle = \sum_j C_j^{\alpha m} |jm\rangle. \quad (7)$$

The mixing amplitudes $C_j^{\alpha m}$ and hence the HF orbits are obtained by solving the HF equation self-consistently

TABLE I. The results of the present experiment and the microscopic Hartree-Fock calculations for different γ transitions in proton quasiparticle $\pi h_{9/2}[541]1/2^-$ band in ^{179}Re.

Energy (keV)	Spin (I_i^π)	Lifetime (ps)	Q_t (e b)	Experimental $B(E2)$ (e^2 b^2)	Hartree-Fock $B(E2)$ (e^2 b^2)
285.8	$\frac{17}{2}^-$	$27.0\pm^{0.6}_{0.9}$	$6.5\pm^{0.1}_{0.1}$	$1.39\pm^{0.1}_{0.1}$	1.56
392.8	$\frac{21}{2}^-$	$4.8\pm^{0.4}_{0.5}$	$6.5\pm^{0.3}_{0.3}$	$1.43\pm^{0.2}_{0.2}$	1.58
483.6	$\frac{25}{2}^-$	$2.1\pm^{0.3}_{0.4}$	$6.5\pm^{0.4}_{0.4}$	$1.45\pm^{0.3}_{0.3}$	1.59
559.2	$\frac{29}{2}^-$	$1.0\pm^{0.2}_{0.2}$	$6.5\pm^{0.4}_{0.5}$	$1.44\pm^{0.3}_{0.2}$	1.59
618.4	$\frac{33}{2}^-$	<1.0	>6.6	>1.53	1.60

TABLE II. The results of the present experiment and the microscopic Hartree-Fock calculations for different γ transitions in both positive ($\alpha=+1/2$) and negative ($\alpha=-1/2$) signature partners in proton quasiparticle $\pi d_{5/2}[402]5/2^+$ band in ^{179}Re.

Signature (α)	Energy (keV)	Spin I_i^π	Lifetime (ps)	Q_t (e b)	Experimental $B(E2)$ (e^2 b^2)	Hartree-Fock $B(E2)$ (e^2 b^2)
	397.3	$\frac{13}{2}^+$	$6.3\pm^{0.5}_{0.4}$	$5.6\pm^{0.2}_{0.3}$	$1.03\pm^{0.1}_{0.1}$	0.90
+1/2	489.5	$\frac{17}{2}^+$	$2.3\pm^{0.1}_{0.1}$	$5.9\pm^{0.2}_{0.2}$	$1.20\pm^{0.1}_{0.1}$	1.12
	547.7	$\frac{21}{2}^+$	<1.3	>5.9	>1.22	1.23
	341.7	$\frac{11}{2}^+$	$16.4\pm^{1.2}_{1.6}$	$5.2\pm^{0.2}_{0.2}$	$0.86\pm^{0.1}_{0.1}$	0.72
−1/2	447.9	$\frac{15}{2}^+$	$4.5\pm^{0.3}_{0.3}$	$5.4\pm^{0.2}_{0.2}$	$0.96\pm^{0.2}_{0.1}$	1.02
	522.7	$\frac{19}{2}^+$	<1.7	>5.9	>1.18	1.20

[17,18]. An intrinsic state $|\phi_K\rangle$ is a Slater determinant of such deformed orbits and is obtained from the HF configuration by appropriate particle-hole arrangement near the proton and neutron Fermi surfaces (actually product of two Slater determinants for protons and neutrons). A given intrinsic state $|\phi_K\rangle$ does not have a unique angular momentum quantum number and is a superposition of various J states [intrinsic states are states of good K but not of good J, angular momentum quantum number of a single-particle orbit is denoted by j. Angular momentum operator for the whole nucleus (i.e., all the active protons and neutrons) is denoted by J]:

$$|\phi_K\rangle = \sum_J C_K{}^J |\Psi_{JK}\rangle \tag{8}$$

The nuclear Hamiltonian is rotationally invariant and physical states should be states of good J. We obtained states of good J by angular momentum (J) projection. By angular momentum projection from these intrinsic states the spectra and other spectroscopic properties (transition rates) can be obtained. The J projection operator is [17]

$$P_K^{JM} = \frac{2J+1}{8\pi^2} \int d\Omega D^{J*}_{MK}(\Omega) R(\Omega). \tag{9}$$

Here $R(\Omega)$ is the rotation operator ($e^{-i\alpha J_z} e^{-i\beta J_y} e^{-i\gamma J_z}$) and Ω stands for the Euler angles (α, β, γ). For intrinsic states with axial symmetry, two of the Euler angles α, γ are integrated out and we are left with the integrals for the kernels for the Euler angle β.

The matrix element of the Hamiltonian between projected states of angular momentum J obtained from intrinsic states ϕ_{K_1} and ϕ_{K_2} is

$$H^J_{K_1K_2} = \frac{2J+1}{2} \frac{1}{(N^J_{K_1K_1} N^J_{K_2K_2})^{1/2}} \int_0^\pi d\beta \sin\beta d^J_{K_1K_2}(\beta) \times \langle \phi_{K_1} | H e^{-i\beta J_y} | \phi_{K_2} \rangle. \tag{10}$$

Here

$$N^J_{K_1K_2} = \frac{2J+1}{2} \int_0^\pi d\beta \sin\beta d^J_{K_1K_2}(\beta) \langle \phi_{K_1} | e^{-i\beta J_y} | \phi_{K_2} \rangle \tag{11}$$

is the amplitude overlap for angular momentum J.

Reduced matrix elements of tensor operator T^L of rank L are given by

TABLE III. The results of the present experiment and the microscopic Hartree-Fock calculations for different γ transitions in both positive ($\alpha=+1/2$) and negative ($\alpha=-1/2$) signature partners in proton quasiparticle $\pi h_{11/2}[514]9/2^-$ band in ^{179}Re.

Signature (α)	Energy (keV)	Spin I_i^π	Lifetime (ps)	Q_t (e b)	Experimental $B(E2)$ (e^2 b^2)	Hartree-Fock $B(E2)$ (e^2 b^2)
	359.6	$\frac{13}{2}^-$	$11.7\pm^{0.8}_{0.9}$	$5.6\pm^{0.2}_{0.2}$	$0.99\pm^{0.2}_{0.2}$	0.61
+1/2	458.9	$\frac{17}{2}^-$	$3.4\pm^{0.3}_{0.4}$	$5.9\pm^{0.3}_{0.3}$	$1.13\pm^{0.2}_{0.1}$	0.93
	534.4	$\frac{21}{2}^-$	$1.9\pm^{0.3}_{0.5}$	$5.3\pm^{0.5}_{0.5}$	$0.94\pm^{0.2}_{0.2}$	1.16
	579.6	$\frac{25}{2}^-$	<0.9	>6.1	>1.29	1.24
−1/2	411.9	$\frac{15}{2}^-$	$7.1\pm^{0.6}_{0.7}$	$5.3\pm^{0.2}_{0.2}$	$0.92\pm^{0.2}_{0.1}$	0.77
	498.9	$\frac{19}{2}^-$	$2.4\pm^{0.2}_{0.2}$	$5.5\pm^{0.2}_{0.2}$	$1.03\pm^{0.1}_{0.1}$	1.05

TABLE IV. Comparison of the experimental and the TRS calculated Q_t values at different rotational frequencies for different ground state bands observed in ^{179}Re.

Band	Experimental value		TRS value			
	$\hbar\omega$ (MeV)	Q_t (e b)	$\hbar\omega$ (MeV)	β	γ	Q_t (e b)
	0.143	6.5±0.1	0.14	0.27	0.6	6.9
$\pi h_{9/2}[541]1/2^-$	0.196	6.5±0.3	0.20	0.27	1.2	6.9
$(-,+1/2)$	0.242	6.5±0.4	0.24	0.26	0.8	6.7
	0.280	6.5±0.4	0.28	0.26	0.5	6.7
	0.309	⩾6.6	0.32	0.25	0.4	6.5
	0.199	5.6±0.3	0.20	0.24	−1.7	6.3
$\pi d_{5/2}[402]5/2^+$	0.245	5.9±0.2	0.24	0.23	−4.0	5.9
$(+,+1/2)$	0.274	⩾5.9	0.28	0.22	−2.5	5.9
	0.171	5.2±0.2	0.18	0.22	−0.3	6.0
$\pi d_{5/2}[402]5/2^+$	0.224	5.4±0.2	0.22	0.23	1.2	6.2
$(+,-1/2)$	0.261	⩾5.9	0.26	0.21	−0.7	5.8

$$\langle \Psi^{J_1}_{K_1} || T^L || \Psi^{J_2}_{K_2} \rangle = \frac{1}{2} \frac{(2J_2+1)(2J_1+1)^{1/2}}{(N^{J_1}_{K_1K_1} N^{J_2}_{K_2K_2})^{1/2}} \sum_{\mu\nu} C^{J_2 L J_1}_{\mu\nu K_1} \int_0^\pi d\beta \times \sin(\beta) d^{J_2}_{\mu K_2}(\beta) \langle \phi_{K_1} | T^L_\nu e^{-i\beta J_y} | \phi_{K_2} \rangle, \quad (12)$$

where T^L is the symbol of electromagnetic operators ($E2$, $M1$, etc.) and K_1,K_2 are axial quantum numbers. The Hamiltonian and kernels of the various quantities are calculated with 64 points Gauss-Legendre quadrature formula. In general, two states $|\Psi^{JM}_1\rangle$ and $|\Psi^{JM}_2\rangle$ projected from two intrinsic configurations $|\phi_{K_1}\rangle$ and $|\phi_{K_2}\rangle$ are not orthogonal to each other even if $|\phi_{K_1}\rangle$ and $|\phi_{K_2}\rangle$ are orthogonal. Whenever necessary we orthonormalize them and then diogonalize using

$$\sum_{K'} (H^J_{KK'} - E N^J_{KK'}) C^J_{K'} = 0. \quad (13)$$

Here $C^J_{K'}$ is the orthonormalized amplitude, which can be identified as the band mixing amplitudes.

The $B(E2)$ values are calculated from the reduced matrix elements of the electric quadrupole moment operator [21] using the following relation:

$$B(E2; \alpha J_1 \to \beta J_2) = \frac{1}{(2J_1+1)} |e^p_{eff} \langle \Psi^{\beta J_2}_{K_2} || Q^p_2 || \Psi^{\alpha J_1}_{K_1} \rangle + e^n_{eff} \langle \Psi^{\beta J_2}_{K_2} || Q^n_2 || \Psi^{\alpha J_1}_{K_1} \rangle|^2. \quad (14)$$

To include the effect of core excitation (core polarization) the effective charges of 1.55e and 0.55e for protons and neutrons, respectively, are used in the above relation. To calculate the $B(M1)$ values for γ transitions from initial state "αI_1" to final state "βI_2" for the rotational bands with $K=5/2$ and $K=9/2$, the following relation is used:

$$B(M1; \alpha J_1 \to \beta J_2) = \frac{3}{(2J_1+1)} \frac{1}{4\pi} \times \left| \sum_{i=p,n} \langle \Psi^{\beta J_2}_{K_2} || g_{l_i} l_i + g_{s_i} s_i || \Psi^{\alpha J_1}_{K_1} \rangle \right|^2, \quad (15)$$

where "g_l" and "g_s" are the orbital and the spin g factors. In the calculations the quenching of spin g factors of half [22] is considered.

IV. DISCUSSION

According to Table I, the average experimental Q_t value for the ground state band built on the $h_{9/2}[541]1/2^-$ is 6.5 e b while the average value for the $d_{5/2}[402]5/2^+$ and for the $h_{11/2}[514]9/2^-$ bands is ~5.6 e b as shown in Tables II and III, respectively. The average experimental Q_t value for the $h_{9/2}$ band is therefore ~16% higher than the average Q_t values for the $d_{5/2}$ and $h_{11/2}$ bands. Although the quadrupole moment of individual states in different bands may not be so different within experimental errors, but the difference of

TABLE V. Single-particle energies (MeV) and the effective charges of protons and neutrons used in the projected HF calculations.

Proton orbitals	$g_{7/2}$	$d_{5/2}$	$d_{3/2}$	$s_{1/2}$	$h_{11/2}$	$h_{9/2}$	$f_{7/2}$	$i_{13/2}$	$g_{9/2}$	e^{eff}_p
Energy	−6.92	−5.56	−3.58	−3.298	−4.376	1.0	2.0	3.0	5.5	1.55e
Neutron orbitals	$h_{9/2}$	$f_{7/2}$	$f_{5/2}$	$p_{3/2}$	$p_{1/2}$	i_{13}	$i_{11/2}$	$g_{9/2}$	$j_{15/2}$	e^{eff}_n
Energy	−11.793	−10.949	−8.407	−8.739	−7.776	−9.494	−4.049	−3.485	−0.95	0.55e

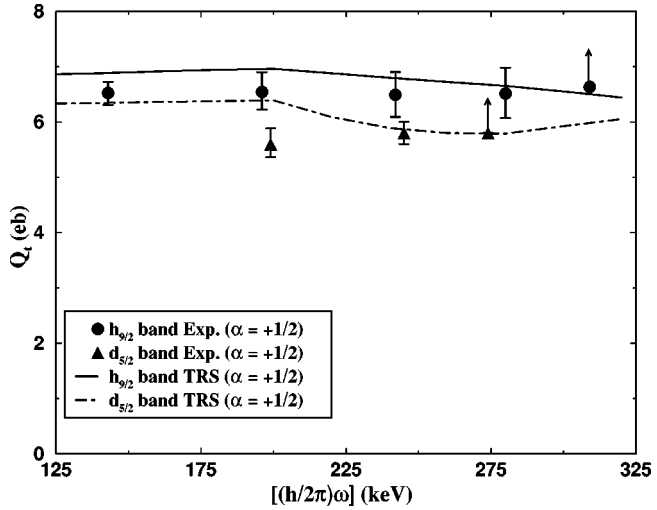

FIG. 5. A comparison of the experimental and the theoretical (TRS) transition quadrupole moments at different rotational frequencies for the positive signature ($\alpha=+1/2$) $\pi h_{9/2}[541]1/2^-$ and the $\pi d_{5/2}[402]5/2^+$ bands in ^{179}Re. The solid and the dot-dash curves are the results of the TRS calculations.

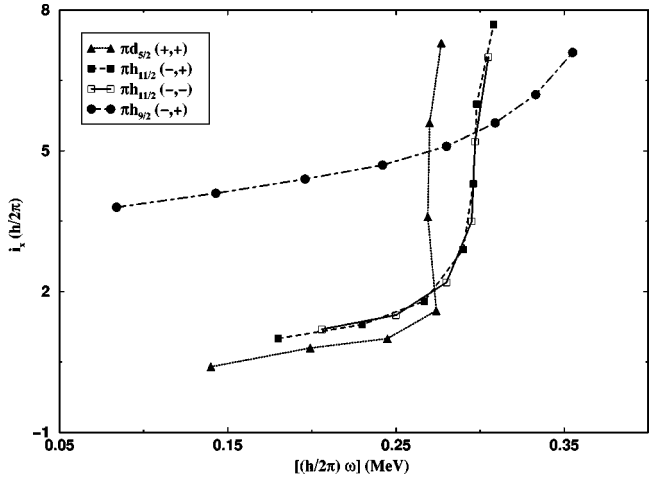

FIG. 6. The plot of the experimental aligned angular momentum I_x as a function of rotational frequency $\hbar\omega$ for different quasiproton bands in ^{179}Re nucleus. (Data are taken from Ref. [6].)

$\sim$16% in the average values does indicate that the core polarization effect generated by the occupation of this high-j, low K $h_{9/2}[541]1/2^-$ orbital by the odd particles has been observed in some other known cases [2–5]. The most expected reason for this quenching of deformation driving property of this high-j, low K $\pi h_{9/2}$ orbital is the effect of Fermi level. In case of Ta, Lu, Ho, and other lighter rare earth nuclei the Fermi surface is below the $\pi h_{9/2}$ shell and hence this acts as a pure particle state and therefore has large deformation driving property. On the other hand in Re nuclei because of the increase of the Fermi level the $\pi h_{9/2}$ shell is near the Fermi surface and therefore has quasiparticle nature with less deformation driving tendency. The transition quadrupole moments Q_t are calculated from the β_2 values obtained from the TRS calculations using Eq. (5) for the ground state negative parity $h_{9/2}$ ($K=5/2$) and the positive parity $d_{5/2}$ ($K=5/2$) band. These are plotted in Fig. 5 as a function of rotational frequency along with the experimental values. At lower rotational frequencies the TRS Q_t values are slightly higher than the experimental values while at higher excitations these are in agreement with the experimental values. The experimental $B(E2)$ values tabulated in Tables I–III also indicate the higher value for $h_{9/2}$ band as compared to $d_{5/2}$ and $h_{11/2}$ bands. The $B(E2)$ values for all three bands are found to remain almost constant as a function of spin. This shows that these bands have no major interaction with other bands in their vicinity so as to keep the deformation sustained as a function of spin till $\hbar\omega \leqslant 0.30$ MeV. The constant nature of experimental $B(E2)$ values with spin is also supported by the microscopic Hartree-Fock calculations.

It is observed from the TRS calculations that for the $h_{9/2}$ band at low frequency the β_2 deformation is high ($\sim$0.25) while the triaxiality parameter γ is $\sim 0°$. With increase in rotational frequency the β_2 deformation for this band increases slightly with no significant change in γ, indicating a stable prolate shape for this configuration. On the other hand for the $d_{5/2}$ band the β_2 and γ values are almost similar to that of the $h_{9/2}$ band at low rotational frequency, while on increasing the spin, β_2 does not show any significant change in its value but the triaxiality γ increases slightly towards the negative γ value ($\gamma \sim -5°$) at $\hbar\omega=0.24$ MeV, indicating the γ-soft nature of the potential for this configuration at higher excitations.

The experimental alignment plots [7] for different quasiproton bands in ^{179}Re in Fig. 6 indicate that for the $[402]5/2^+$ and $[514]9/2^-$ bands the initial alignment is small ($\sim 1\hbar$) but with increasing rotational frequency a clear upward bending with a sharp gain in alignment ($\sim 7.5\hbar$) is seen at a rotational frequency of $\hbar\omega \sim 0.26$ MeV. The small initial alignment at low frequencies for these two high K bands is because of their deformation aligned nature at small frequencies. This is indicated by the high $B(M1)$ values at low frequency for these two bands. With increase in rotation, as the odd proton starts aligning its dipole axis (spin axis) from deformation axis towards the rotation axis, these bands become more and more rotational aligned and hence smooth gain of alignment is observed. This effect is clearly seen with the decrease in the $B(M1)/B(E2)$ ratio with spin for the two bands in Fig. 7. Since for both the bands the $B(E2)$ values are almost constant, the decrease in the ratio is mainly because of decrease in $B(M1)$ values with rotation as predicted by the microscopic Hartree-Fock calculations. The sharp gain in alignment for these two bands at $\hbar\omega \sim 0.26$ MeV is because of the crossing of these bands with the intersecting three quasiparticle bands formed by the decoupling of an $i_{13/2}$ neutron pair at this particular frequency. On the other hand, as the $h_{9/2}[541]1/2^-$ band arises from the high-j orbital which is strongly affected by the Coriolis force and therefore more rotational aligned, a comparatively large initial alignment ($\sim 4\hbar$) is observed at small rotational frequencies. On increasing the rotational frequency a smooth gain in alignment is observed up to $\hbar\omega \sim 0.3$ MeV. This $[541]1/2^-$ configuration shows the first band crossing at $\hbar\omega=0.33$ MeV, a value much larger than that of the $[402]5/2^+$ and $[514]9/2^-$ bands ($\hbar\omega \sim 0.26$ MeV). This difference of $\sim$70 keV in the

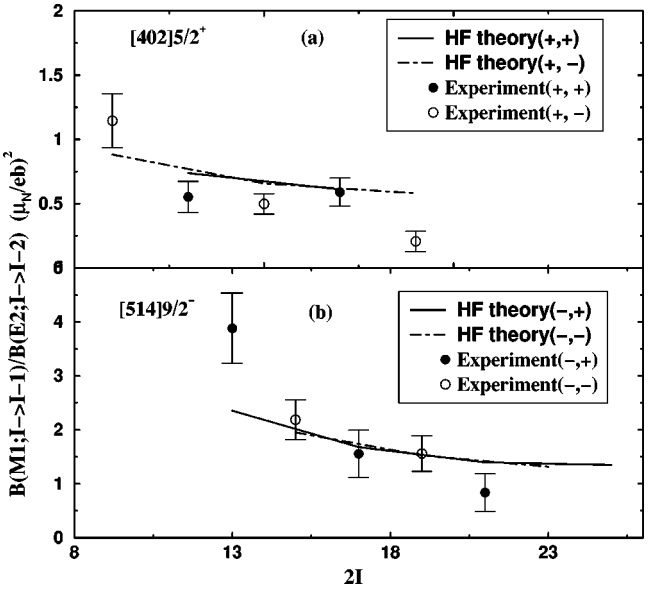

FIG. 7. The plot of the $B(M1)/B(E2)$values with spin I for the strongly coupled (a) positive parity $\pi d_{5/2}$ band and (b) negative parity $\pi h_{11/2}$ band in ^{179}Re. The solid and the dot-dash curves are the results of the projected HF microscopic calculations. On the x axis the spins are represented in the units of $\hbar$.

crossing frequency for the $K=1/2$ band as compared to the higher K bands has been observed in ^{177}Re [23] and ^{171,173}Ta [24] nuclei also. The most expected reason for this delay in the band crossing frequency for this low K, high-j $[541]1/2^-$ band compared to the other bands in the same nucleus and also compared to the ground state band in neighboring even-even nuclei is mainly because of the large quadrupole deformation of this band. The high value of quadrupole pairing interaction prevents the alignment of $\nu i_{13/2}$ neutron pair from occurring so early. This has been confirmed from the lifetime measurements in ^{171,173}Ta [2,3] and ^{177}Re [4] as being due to the deformation driving nature of the low K, high-j $h_{9/2}$ configuration. In the case of ^{177}Re nucleus [23] this $[541]1/2^-$ band shows a pronounced backbending at almost the same rotational frequency $\hbar\omega=0.33$ MeV, so if the higher deformation of this band is responsible for the shifting of the band crossing frequency to higher values then the similar shift of $\sim$70 keV for $[541]1/2^-$ band in ^{177}Re and ^{179}Re indicates that in this configuration the two nuclei should have nearly the same deformation. This is actually being verified as the average value of transition quadrupole moment Q_t in this case is found to be the same as in ^{177}Re [4] with the mean values of 6.5 e b. The nearly same value of the transition quadrupole moments in the two rhenium isotopes with neutron numbers $N=102$ and 104 indicates the stability of nuclear shape for the ground state configuration around the neutron midshell ($N=104$) as predicted in the theoretical studies done by Nazarewicz *et al.* [25].

V. SUMMARY

The deformation driving properties of the low K, $\pi h_{9/2}[541]1/2^-$ band and the high K, $\pi d_{5/2}[402]5/2^+$ and $\pi h_{11/2}[514]9/2^-$ bands are discussed on the basis of the results obtained from the RDM lifetime measurements in ^{179}Re. The theoretical Q_t values obtained from the TRS calculations and the $B(E2)$ values obtained from the microscopic Hartree-Fock calculations are compared with the experimental values for these configurations. The average quadrupole moment for the $[541]1/2^-$ band is found to be $\sim$16% higher than the $[402]5/2^+$ and $[514]9/2^-$ bands, indicating the deformation driving nature of this low K, high-j $h_{9/2}$ band. The Q_t values derived from the TRS calculations for the negative and the positive parity ground state $h_{9/2}$ and $d_{5/2}$ bands agree qualitatively with the experimental observations. The slight increase in the triaxiality parameter γ from 0° to −5° as a function of the rotational frequency for the $d_{5/2}$ band indicates the γ softness for this configuration. The constant nature of the $B(E2)$ values with the increase in the rotational frequency ($\hbar\omega\sim0.30$ MeV) for the $h_{9/2}$ ($K=1/2$), $d_{5/2}$ ($K=5/2$), and $h_{11/2}$ ($K=9/2$) bands indicates the stability of the nuclear shape for this nucleus. The $B(E2)$ values obtained from the microscopic HF calculations are found to be in close agreement with the experimental $B(E2)$ values for these bands. The observed gradual increase in the alignments with the increase in the rotational frequency for the ground state $h_{11/2}$ and the $d_{5/2}$ bands results in the corresponding decrease in the $B(M1)/B(E2)$ ratio which is well explained within the framework of the projected HF calculations [24,25].

ACKNOWLEDGMENTS

The authors would like to thank the Pelletron crew at Nuclear Science Center, New Delhi for providing the good quality beam during the experiment. We are also thankful to UGC and CSIR, India for providing financial support for this experiment.

[1] H. Q. Jin *et al.*, Phys. Rev. C **53**, 2106 (1996).
[2] P. Joshi *et al.*, Phys. Rev. C **60**, 034311 (1999).
[3] P. Joshi *et al.*, Phys. Rev. C **64**, 034303 (2001).
[4] S. K. Chamoli *et al.*, Phys. Rev. C **66**, 024307 (2002).
[5] D. Muller *et al.*, Phys. Lett. B **332**, 265 (1994).
[6] K. Walus *et al.*, Phys. Scr. **34**, 710 (1986).
[7] Ts. Venkova *et al.*, Z. Phys. A **334**, 385 (1989).
[8] S. K. Chamoli *et al.*, Nucl. Phys. **A722**, 563c (2003); see also *Proceedings of the ISPUN02 Conference*, Vietnam, edited by Dao Tien Khoa, Nguyen Dinh Dang, and Shegeru Kubono (Elsevier Sciences, Amsterdam, North Holland, 2003), p. 563c.
[9] T. K. Alexander and A. Bell, Nucl. Instrum. Methods **81**, 22 (1970).
[10] J. C. Wells *et al.*, Report No. ORNL/TM-9105, 1985.

[11] A. Abragam and R. V. Pound, Phys. Rev. **92**, 943 (1953).
[12] F. James and M. Roos, Comput. Phys. Commun. **10**, 343 (1975).
[13] R. Bengtsson and J. D. Garrett, in *International Review of Nuclear Physics*, edited by T. England *et al.* (World Scientific, Singapore, 1984), Vol. 2.
[14] V. M. Strutinsky, Nucl. Phys. **A95**, 420 (1967).
[15] T. R. Werner and J. Dudek, At. Data Nucl. Data Tables **50**, 172 (1992).
[16] S. G. Nilsson and I. Rangarsson, *Shapes and Shells in Nuclear Structure* (Cambridge University Press, Cambridge, 1995), p. 290.
[17] G. Ripka, in *Advance in Nuclear Physics*, edited by M. Baranger and E. Vogt (Plenum, New York, 1966), Vol. 1, p. 183.
[18] C. R. Praharaj and S. B. Khadkikar, Phys. Rev. Lett. **50**, 1254 (1983).
[19] C. R. Praharaj, J. Phys. G **14**, 843 (1988).
[20] A. Faessler *et al.*, Phys. Rev. **156**, 1067 (1967).
[21] I. Talmi, *Simple Models of Complex Nuclei* (Harwood Academic, Chur, Switzerland, 1993), p. 166.
[22] A. Bohr and B. R. Mottelson, *Nuclear Structure*, Vol. 2 (World Scientific, Singapore, 1975).
[23] R. A. Bark *et al.*, Nucl. Phys. **A591**, 265 (1995).
[24] J. C. Bacelar *et al.*, Nucl. Phys. **A442**, 547 (1985).
[25] W. Nazarewicz, M. A. Riely, and J. D. Garrett, Nucl. Phys. **A512**, 61 (1990).